Atomization and Sprays, x(x): 1–24 (2017)

FROM HIGH-FIDELITY NUMERICAL SIMULATIONS OF A LIQUID FILM ATOMISATION TO A REGIME CLASSIFICATION

Camille Bilger & R. Stewart Cant*

Department of Engineering, University of Cambridge, Trumpington street, CB2 1PZ, Cambridge, United Kingdom

*Address all correspondence to: Camille Bilger, E-mail: cb757@cam.ac.uk

Original Manuscript Submitted: ; Final Draft Received:

High-fidelity numerical simulations of spray formation were conducted with the aim of improving fundamental understanding of airblast liquid film atomisation. The gas/liquid interaction in the near nozzle region is investigated for a multitude of operating conditions in order to extrapolate phenomenological and breakup predictions. To reach this goal, the Robust Conservative Level Set (RCLS) method has been used. For a fixed prefilmer geometry, we performed a parametric study on the impact of various liquid and gas velocities on the topological evolution of the liquid interface. The behaviour and development of the liquid film is found to be influenced mainly by the relative inertia of the gas and the liquid, the liquid surface tension and interfacial shear stresses. Preliminary regime maps predicting the prefilming liquid-sheet atomisation behaviour are constructed based on our numerical results. Three distinct types of "regime" are reported: accumulation, ligament-merging and 3-D wave mode. In addition, these results also show the influence of vortex action and rim-driven dynamics on the breakup mechanism at the atomiser edge. An increase in liquid injection speed leads to the generation of smaller droplets whereas an increase in air velocity does not point to one simple conclusion.

KEY WORDS: *primary atomization; airblast; liquid film; conservative level-set; RCLS method; incompressible flow; multiphase flow*

1. INTRODUCTION

The numerical simulation of atomising liquid films has become a major topic of interest, answering the need to enhance engine efficiency and reduce polluting agents. However, the physics of the atomisation process involves a wide range of phenomena and strongly multi-scale dynamics, in which a wide variety of liquid structures of different sizes and very different topologies, such as drops and ligaments, are generated as a consequence of the many hydrodynamic instabilities which arise. The complexity of the problem is due to this chain of physical processes involved in parallel and/or in sequence. The detailed numerical simulation of aeronautical combustion chambers at realistic operating conditions is thus an extremely complex calculation. The aim of the present research is to advance fundamental understanding of the process by isolating simplified and small-scale configurations and attempting to extract features that yield physical insight into the mechanisms involved.

A vast amount of literature has accumulated on the subject of spray formation: much progress has been made towards high-order numerical schemes (Desjardins, 2008; Kim and Moin, 2011; Pringuey and Cant, 2012, 2014; Zuzio et al., 2017), computational power (Cuenot et al., 2016), and experimental visualisations (Déjean et al., 2016;

1044–5110/17/$35.00

Gepperth et al., 2012; Guildenbecher, 2016). In spite of this, many aspects of spray formation are still poorly understood even at standard atmospheric conditions, let alone the requirement for a deeper analysis of the mechanisms and processes involved at engine-relevant operating conditions.

Although a few numerical and experimental studies have been performed on prefilming liquid-sheet atomisation, a combined investigation considering the liquid wall film on top of the prefilmer and its subsequent disintegration is still a missing link, as pointed out by Warncke et al. (2017).

Most authors agree on the critical influence of the relative liquid/gas velocity ratio on the atomisation process and recognise that most atomisation mechanisms are connected with wave formation, wave development and wave disintegration. The question remains as to whether the onset of shear-driven instabilities and surface wave development have an effect on atomisation for every operating condition. Also, the reported effects from surface tension forces and inertial forces are often contradictory. In addition, there is no universal consensus regarding which additional flow parameters and geometrical parameters characterise the breakup process in liquid film configurations. The effects of the physical properties of the liquid and the gas seem to be strongly regime dependent, highlighting the need to continue investigating the physics in different regimes. This leaves the door open for a variety of useful investigations.

The present approach constitutes a systematic fundamental investigation of the physics involved during the atomisation of an airblasted liquid film, described herein, to characterise the primary breakup mechanisms and the dominating liquid deformations. We perform high-fidelity transient three-dimensional calculations for a parametric range of liquid and gas injection velocities, providing detailed information on the processes and structures in the near nozzle region.

The paper is organised as follows. Section 2 presents the RCLS method for the computation of primary atomisation. Section 3 details the computational settings employed in the simulation of the atomisation of a prefilming airblasted liquid film, in particular, the mechanical and physical boundary and initial conditions. In Section 3.1 and 3.2 we discuss briefly the implications of our choice in numerical resolution and flow physical condition. In Section 4 and 5 we present the results of our high-fidelity numerical simulations and regime cartography exercise. Finally, in Section 6 we discuss the implications of the inter-phase competition for inertia and surface tension-driven atomisation mechanisms, before drawing some conclusions in Section 7.

2. NUMERICAL METHOD

The motion of the fluid is governed by the Navier–Stokes equations,

$$\frac{\partial \rho \mathbf{u}}{\partial t} + \nabla \cdot (\rho \mathbf{u}\mathbf{u}) = \nabla \cdot \mathcal{T} + \mathbf{f} \qquad (1)$$
$$\nabla \cdot \mathbf{u} = 0$$

with constant densities ρ_{gas} and ρ_{liq} and viscosities μ_{gas} and μ_{liq}, and where $\mathbf{u}$ is the fluid velocity and $\nabla \cdot \mathcal{T}$ is the viscous stress tensor: $\mathcal{T} = -p\mathcal{I} + \mu\mathcal{S}$, where p is the pressure, $\mathcal{I}$ is the identity tensor, and $\mathcal{S}$ is the strain rate tensor defined as

$$\mathcal{S} = (\nabla \mathbf{u})^T + (\nabla \mathbf{u}). \qquad (2)$$

The term $\mathbf{f} = \mathbf{f_g} + \mathbf{f_c}$ corresponds to all the external forces, where $\mathbf{f_g} = \rho \mathbf{g}$ is the gravitational force. The velocity field is continuous across the sharp interface Γ in the absence of phase change. However, the existence of surface tension forces will lead to discontinuous normal stresses at the phase interface. This results in an interfacial jump in pressure, expressed as the Young-Laplace junction condition

$$[-p\mathbf{I} + \mathbf{S}]_\Gamma \cdot \hat{\mathbf{n}}_\Gamma = \sigma\kappa\hat{\mathbf{n}}_\Gamma \qquad (3)$$

for constant σ along the interface. The normal to the interface is $\hat{\mathbf{n}}_\Gamma$, κ its curvature and σ the surface tension coefficient. The source term $\mathbf{f_c}$ effectively represents the singular capillary forces, present only on the nearly infinitely thin interface.

2.1 Conservative level-set approach with WENO treatment of the transport equation for the phase interface

The implicit interface-capturing approach within the mass-conservative RCLS method of Pringuey and Cant (2014) is based on the conservative level-set method (CLS) of Olsson and Kreiss (2005) Olsson et al. (2007). Instead of transporting a signed distance function ϕ as for the classic level-set methods (Sussman et al., 1994), conservative level-set methods transport a hyperbolic tangent function $\psi(\mathbf{x}, t)$ that can be initialised with the signed distance function ϕ as follows:

$$\psi = \frac{1}{2}\left(\tanh(\frac{\phi}{2\epsilon}) + 1\right). \tag{4}$$

The hyperbolic tangent level-set function ψ has for phase interface definition the iso-surface $\psi = 0.5$.

In Equation 4, ϵ is introduced by Olsson and Kreiss (2005) as a control parameter over the thickness of the interface, which is kept constant once defined. Olsson and Kreiss (2005) recommend $\epsilon = \overline{\Delta x}/2$, where $\overline{\Delta x}$ is the average mesh spacing.

The Continuum Surface Force (CSF) method of Brackbill et al. (1992), in which the capillary forces are treated as volumetric surface tension forces:

$$\mathbf{f_c} = \sigma\kappa\nabla\psi. \tag{5}$$

The interface curvature is given by

$$\kappa = -(\nabla \cdot \hat{\mathbf{n}}_\Gamma) \tag{6}$$

and the interface normal $\hat{\mathbf{n}}_\Gamma$ by

$$\hat{\mathbf{n}}_\Gamma = \frac{\nabla\psi}{|\nabla\psi|}. \tag{7}$$

According to the CSF method, the material properties over the whole multiphase domain are given by:

$$\begin{aligned} \rho &= \rho_{\text{gas}} + (\rho_{\text{liq}} - \rho_{\text{gas}})\psi \\ \mu &= \mu_{\text{gas}} + (\mu_{\text{liq}} - \mu_{\text{gas}})\psi \end{aligned} \tag{8}$$

The conservative level-set ψ is advected in a zero-divergence velocity field

$$\frac{\partial\psi}{\partial t} + \nabla \cdot (\mathbf{u}\psi) = 0 \tag{9}$$

in a conservative manner such that it remains conserved to machine accuracy. Equation 6 is solved with an arbitrarily high-order WENO scheme for unstructured meshes with 3-D mixed-elements, as detailed in Pringuey and Cant (2012). In addition, the complexity of high-order schemes was handled efficiently by ensuring that as much as possible of the computational work was done through pre-processing operations, in order to reduce the work done at run-time. The latter is explained in detail in Pringuey and Cant (2012).

A re-initialisation algorithm is applied to ensure mass-conservation to machine accuracy, as detailed in Pringuey and Cant (2014). This is because even high-order numerics such as the WENO scheme will eventually diffuse the interface. The level set profile ψ needs to recover its original hyperbolic tangent shape and maintain a constant interface thickness.

$$\frac{\partial\psi}{\partial\tau} + \nabla \cdot (\psi(1-\psi)\hat{\mathbf{n}}_\Gamma) - \epsilon\nabla \cdot (\nabla\psi) = 0 \tag{10}$$

where τ is the artificial time along which the equation is solved until the initial conservative level-set profile is recovered, and $\hat{\mathbf{n}}_\Gamma$ is the normal to the interface. The formulation presented is combining the simplicity and generality of the original re-initialisation equation by Sussman et al. (1994) in terms of high-order standard discretisation and the accuracy of the constrained re-initialisation scheme in terms of interface displacement.

A third-order Runge–Kutta (RK) scheme for temporal discretisation is used for both the advection (Equation 6) and re-initialisation steps (Equation 7).

The RCLS method is implemented within the open source CFD software package OpenFoam® (Weller et al., 1998) from which the default Multidimensional Universal Limiter with Explicit Solution (MULES) is employed to maintain the boundedness of the liquid volume fraction profile. The addition of the flux limiter guarantees that the liquid volume fraction remains physical everywhere in the computational domain ($0 < \psi < 1$). In addition, the pressure-velocity coupling is handled within the framework of OpenFoam using the standard Pressure Implicit with Splitting of Operators (PISO) method by Issa (1985). A n-halo parallelisation method has been implemented in OpenFoam to perform the computations at the required order of accuracy, as detailed in Pringuey and Cant (2012). The resulting method was demonstrated in Pringuey and Cant (2014). More recently, the same approach was tested for multiphase flows in low-capillary number environments (Bilger et al., 2017).

3. SETTINGS OF THE COMPUTATIONS

The real annular geometry of most airblast commercial atomisers is simplified into a three-dimensional planar geometry (Fig. 1), where the liquid is injected as a thin planar sheet. Our computational domain is a cuboid of $16 \times 11 \times 4$ mm^3, where the prefilmer is a flat solid plate of 8mm in length, 1mm thickness and 4mm in width. The x-direction corresponds to the streamwise direction, the y-direction is upward and the z-direction is spanwise. As the emphasis of this numerical study is placed on the mechanisms driving primary breakup, the computational domain is limited to the close vicinity of the injection plane: we resolve a length downstream of the prefilmer plate of 8mm. Our choice for dimensions is based on commonly-used injector geometries for experimental studies of prefilming airblast atomisation and on how large the perturbations of the liquid film are expected to be. The front and back planes are set as cyclic boundary conditions. The rest of the domain boundaries are defined as inlet/outlet boundary conditions, fixed mass inflow and fixed back pressure. The RCLS method is designed to run on hybrid meshes. However, to improve

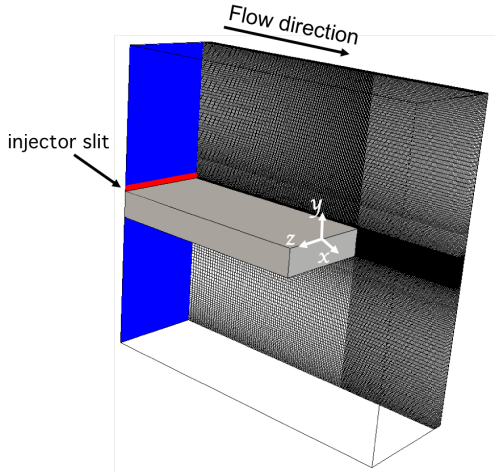

FIG. 1: Mid-plane cut of the mesh with the liquid rectangular inlet slit shown in red, the gas inlet planes in blue and the prefilmer (rectangular parallelepiped) in grey.

the accuracy in representing the atomisation process, the entire computational domain is meshed with 2.47×10^6 hexahedral elements. The RCLS method with WENO treatment of the phase interface advection requires 5 points in any one direction of the WENO stencils (Bilger et al., 2017; Pringuey and Cant, 2014). As a result, the liquid film height comprises 5 mesh elements for full numerical resolution. The simulations were carried out on the Cambridge HPC cluster, which consists of 9600 2.60GHz Intel Sandy Bridge cores connected by Mellanox FDR Infiniband (600 nodes, 64GB of RAM per 16-cores node). A typical simulation required about 110 CPU hours on 96 cores (8 nodes) to generate 0.003 seconds of simulated time. The timestep was allowed to vary for numerical stability of the scheme and runtime efficiency, averaging to a value of 1×10^{-7} seconds throughout the simulation, with an imposed

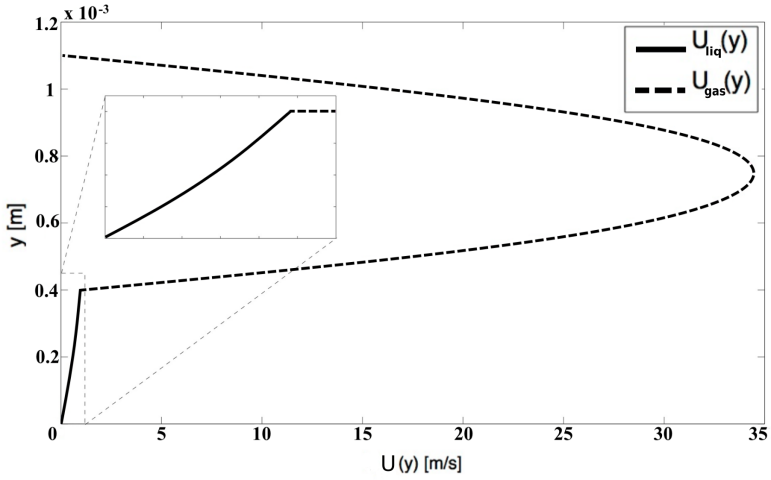

FIG. 2: Example the inflow axial velocity profiles for the top inlet channel, above the prefilmer plate. The liquid velocity is shown as a continuous line and the gas velocity with a dashed line.

maximum CFL number of 0.5.

In multiphase flow dynamics, the timestep must be small enough to resolve the propagation of the capillary waves that develop at the interface (Brackbill et al., 1992). Here we keep the maximum Courant number in the domain under 0.5.

Previous numerical and experimental studies of atomisation have highlighted the sensitivity of computations to boundary conditions on the liquid atomisation. In particular, it is believed that the accurate representation of both velocity profiles (boundary layers in liquid and gas phases) is critical to predict the onset of the breakup and the growth of perturbations at the interface (Kane, 1994; Lozano and Barreras, 2001; Marmottant and Villermaux, 2004). The liquid and the gas both enter the simulation domain at the inlet plane, with different heights $h_{\mathrm{liq}} = 0.1$mm and $h_{\mathrm{gas,top}} = h_{\mathrm{gas,bottom}} = 5$mm; and at different mean velocities $\overline{u}_{\mathrm{liq}}$ and $\overline{u}_{\mathrm{gas}}$. A continuous laminar airflow with no swirl is supplied at the inlet plane. The air emerging is split into two streams that pass the prefilmer on each side. The gas enters the domain with a parabolic velocity profile in each channel in order to account as much as possible for upstream flow development in the air supply channels. The mean air speed is varied parametrically between 5 and 50m/s. The liquid is continuously fed onto the prefilmer plate through an injector slit at the inlet plane of 4mm$\times$0.1mm with a uniform velocity profile and mean speed varied parametrically between 0.5 and 10m/s. The liquid forms a thin film travelling downstream.

We assign a boundary condition generating a small-amplitude fluctuating inlet velocity to the liquid inlet plane by adding a random component to the mean velocity field, in all-three directions, defined as a fraction of the mean velocity, based on a chosen intensity ($\pm 1\%$). This is done to avoid perturbations of the surface in the first instants of the injection being triggered purely by uncontrolled numerical noise. Instead, perturbations are triggered by our own controlled uncorrelated fluctuations.

The liquid stream and top gas stream rapidly develop into a two-phase Poiseuille flow profile, with a point of inflection, as expected, over the course of a few mesh elements (Fig. 2). The flow conditions chosen for this study are listed in Table 1. All numerical simulations use atmospheric conditions for pressure and temperature. Gravity is ignored in the context of primary atomisation as it has no effect over the lengthscales and timescales involved.

The no-slip wall boundary condition, as readily implemented in OpenFoam, was used as part of this investigation. As a result, a static fixed contact angle of 90 has been set for the liquid flowing over the walls of the prefilmer. For a discussion on the implementation of a dynamic contact angle model within the RCLS method, the reader is referrred to Section 7.

Evaporation is neglected because the dense-spray region generally involves relatively cool portions of the flow where rates of heat and mass transfer are modest (Faeth et al., 1995).

TABLE 1: Material properties for the simulation of atomisation

Phase	ρ [kg/m^3]	μ [kg/m.s]	$\overline{u}$ [m/s]	σ [N/m]
Gas	1.2	1.18×10^{-5}	5–50	
Liquid	998	1.0×10^{-3}	0.5–10	0.0283

There is a lack of consensus over the choice of suitable non-dimensional numbers, which highlights the absence of a comprehensive understanding of primary atomisation. We base our choice for non-dimensional groups on the studies of Déjean (2015), Sauer (2014) and Ling et al. (2017). Crucial factors influencing atomisation in configurations typical of airblast atomisers are the density ratio $\rho_{\rm gas}/\rho_{\rm liq}$ and viscosity ratio $\mu_{\rm gas}/\mu_{\rm liq}$. In addition, the relative velocity between the liquid flow and the gas phase $\overline{u}_{\rm gas}/\overline{u}_{\rm liq}$ has a significant impact. A way to combine the effect of density and velocity ratios is to introduce the momentum flux ratio MFR that reads:

$$\mathrm{MFR} = \frac{\rho_{\rm gas}\overline{u}^2_{\rm gas}}{\rho_{\rm liq}\overline{u}^2_{\rm liq}}. \tag{11}$$

Lozano et al. (2005) identified the strong influence of the initial height of both fluid channels and suggested the use of the momentum ratio instead:

$$\mathrm{MR} = \frac{\rho_{\rm gas}\overline{u}^2_{\rm gas}h_{\rm gas}}{\rho_{\rm liq}\overline{u}^2_{\rm liq}h_{\rm liq}} \tag{12}$$

where $h_{\rm gas}$ and $h_{\rm liq}$ are the lengthscales for the gas and liquid, respectively. An important dimensionless group is the Weber number which represents the ratio of the disruptive aerodynamic forces to the restoring surface tension forces:

$$\mathrm{We} = \frac{\rho_{\rm gas}\overline{u}^2_i h}{\sigma} \tag{13}$$

where $\overline{\rm u}_i$ is either taken as the velocity of the gas $\overline{\rm u}_{\rm gas}$ or defined by some authors as $u_{\rm rel}$, the relative velocity between the liquid and the gas-phase (e.g. Sauer et al., 2016). The lengthscale parameter h is often taken as a lengthscale based on a liquid phase scale (e.g. Bhayaraju and Hassa, 2009; Sauer et al., 2016). It seems reasonable to base the choice of the lengthscale h on the height of the liquid injection channel as done by Sauer et al. (2016) and Ling et al. (2017). It is also useful to mention the Reynolds number, expressed as the ratio between the aerodynamic forces and the viscous forces:

$$\mathrm{Re} = \frac{\rho_{\rm gas}\overline{\rm u}_{\rm gas}{\rm h}}{\mu_{\rm gas}}. \tag{14}$$

Another useful dimensionless number is the Ohnesorge number:

$$\mathrm{Oh} = \frac{\mu_{\rm liq}}{\rho_{\rm liq}{\rm h}_{\rm liq}\sigma^{1/2}} \tag{15}$$

which relates the internal viscous force to inertia and surface tension forces. The order of magnitude of the non-dimensional numbers associated with the flows simulated are given in Table 2.

The parameters of the RCLS numerical method have been chosen to reach a trade-off in terms of performance, stability of the method and compliance with the physics of the atomisation. The chosen set of RCLS parameters, discussed in Section 2, is shown in Table 3.

TABLE 2: Non-dimensional numbers investigated in this study. The ranges given correspond to the lowest and highest relative velocity between the two fluids.

$\rho_{\mathrm{liq}}/\rho_{\mathrm{gas}}$	$\mu_{\mathrm{liq}}/\mu_{\mathrm{gas}}$	MFR	MR	Oh	$\mathrm{We}_{\mathrm{gas,h_{liq}}}$	$\mathrm{Re}_{\mathrm{gas,h_{liq}}}$
830	80	0.0075–12	0.37–600	0.0595	0.038–10.39	500–4990

TABLE 3: RCLS parameters for the simulation of atomisation

Order of the polynomial reconstruction:	$r = 3$
Numerical scheme:	WENO
CLS coefficient:	$\epsilon = 0.5\overline{\Delta x}$
Periodicity of re-initialisation:	$N_S = 5$

3.1 Discussion on mesh resolution

In multiphase flows, resolving the interface in a given mesh element, which is of the order of the molecular scale in thickness, is impractical. Nevertheless, the more refined the mesh, the more accurate the resolution of interfacial geometrical properties such as curvature and unit normal. The focus of the present study does not lie in the need to resolve the smallest lengthscales of the flow, but to conduct a wide parametric study with the most affordable mesh to accurately resolve the interface geometrical properties and surface tension forces.

One of the smallest lengthscales associated with the flow field that we aim to resolve is the estimated maximum droplet diameter produced. The finest mesh spacing should therefore be calibrated to capture those liquid structures as the smallest drop size captured will always depend on the smallest mesh spacing used in the computational modelling of multiphase flows. A liquid blob moving in a gaseous phase is subjected to aerodynamic forces, which could lead to its deformation and fragmentation into smaller and smaller droplets (secondary atomisation). From droplet stability studies, the critical condition for drop breakup is reached when the aerodynamic force exerted on the drop is equal to the surface tension force (Lefebvre, 1989). In inertia-dominated flow fields, the critical Weber number is an appropriate criterion for the prediction of the initiation of droplet breakup:

$$\mathrm{We_c} = \frac{\rho_{\mathrm{gas}} u_{\mathrm{rel}}^2 D_{\mathcal{D}}}{\sigma}. \tag{16}$$

where $D_{\mathcal{D}}$ is the droplet diameter. Equation 16 is valid only for low-viscosity liquids, i.e. for very low Ohnesorge numbers (Oh$<$ 0.1). In this respect, the critical Weber number for breakup has been reported to be around 12 by different experimental studies (Guildenbecher et al., 2009; Lefebvre, 1989). The latter allows us to estimate the maximum diameter of stable droplets in a given spray that can be observed right after primary breakup:

$$D_{\mathcal{D},\max} = \frac{\mathrm{We_c}\,\sigma}{\rho_{\mathrm{gas}} u_{\mathrm{rel}}^2}. \tag{17}$$

In our computations, for $\mathrm{W}_c = 12$ and for the highest relative velocity investigated between the two fluid phases, $D_{\mathcal{D},\max} = 100\mu$m. Considering that a given length scale L is resolved if $L \geq 2\overline{\Delta_x}$ (Pringuey, 2012), where $\overline{\Delta_x}$ is the average characteristic length scale of the mesh, it can be seen that the maximum droplet diameter resulting from primary breakup is properly resolved by our mesh, which suggests that the mesh can resolve the smallest liquid structures produced. This further highlights our ability to make an efficient use of mesh cells using the RCLS method.

3.2 Discussion on turbulence

Turbulence is likely to be generated within the liquid phase because of the interfacial shear between the gas and liquid and resulting boundary layer development. Indeed, past studies of pressure-atomised sprays have established that one of the criteria for the development of interfacial structures and the onset of breakup is the presence of turbulence at the jet exit (Faeth et al., 1995). In certain phenomenological atomisation models, turbulent eddies with sufficient kinetic energy to overcome the liquid surface tension are able to deform and disrupt the interface, as described in Som and Aggarwal (2010) and Fuster et al. (2009). In addition, the computational diesel spray atomisation simulations of Bianchi et al. (2005) and de Villiers et al. (2004) have highlighted the sensitivity of computations to turbulent boundary conditions on liquid atomisation.

Turbulence is undoubtedly created during prefilming liquid film primary breakup, simply due to the atomisation dynamics themselves. However its feedback on those same dynamics is poorly understood as a systematic study of this effect has yet to be undertaken. The presence and properties of turbulent boundary layers and level of turbulence along the passage walls are rarely quantified in experimental data on prefilming atomisation, because of the difficulty in experimental measurement.

The question remains whether turbulence in the two-phase system provokes, enhances or suppresses atomisation and whether a laminar environment accompanied by hydrodynamic instabilities is sufficient to result in primary breakup. Older classical primary breakup theories by Taylor (1963) and Levich (1962) showed that aerodynamic forces could contribute solely to the breakup of a (non-turbulent) liquid bulk. As pointed out by Faeth et al. (1995) and more recently by Desjardins (2008), these theories merit additional study.

In the present study, we aimed to separate the growth of perturbations at the interface and subsequent atomisation from any influences due to pre-existing turbulence within the flow. Hence the inflow conditions in the present study are chosen to be laminar.

Furthermore, it is interesting to note that, for a turbulent liquid Weber number defined as $\mathrm{We}_{\mathrm{turb}} = \frac{\rho_{\mathrm{liq}} u'^2 h_{\mathrm{liq}}}{\sigma}$, and assuming a velocity fluctuation of 6% in the liquid phase flowing at 10m/s and the highest possible eddy size to be of the order of the liquid channel height h_{liq}, we recover $\mathrm{We}_{\mathrm{turb}} \sim 1$. The liquid turbulence is therefore unlikely to have an impact on the breakup. In addition, the liquid Reynolds number, $\mathrm{Re}_{\mathrm{liq}} = \frac{\rho_{\mathrm{liq}} \overline{u}_{\mathrm{liq}} h_{\mathrm{liq}}}{\mu_{\mathrm{liq}}}$ is found to be of the order of 990. Given the liquid Reynolds number at play, the liquid flow can be viewed as laminar, as the critical Reynolds number corresponding to the transition between the laminar and turbulent regime is considered to be of the order of 2,500 (Déjean, 2015). Hence, turbulence in the air flow is unlikely to play an important role within the thin and viscous liquid film region.

4. ATOMISATION REGIME MAPPING

Inspired by the recently published works of Bhayaraju and Hassa (2009), Inamura et al. (2012), Lozano et al. (2011) and Déjean et al. (2016), which have worked towards the elaboration of regime classifications for atomisation of planar liquid films, the present study sets out to propose a cartography for prefilming liquid film atomisation based on the gas and liquid injection velocities.

Fig. 3 shows the results of the set of high-fidelity numerical simulations that were conducted with the RCLS method, at ambient pressure and temperature. A schematic preliminary regime diagram is built based on the key findings presented in the following sections (Fig. 4).

We considered it convenient in the first instance to present these results in a dimensional space to facilitate comparisons with experimental results, where in general variables such as liquid and gas loading rather than non-dimensional groups are directly controlled.

For very low liquid flow rates ($\overline{u}_{\mathrm{liq}} = 0.5$m/s), liquid accumulates at the atomising edge and experiences deformation by which an intermittent liquid release occurs. The liquid structures and droplets generated are rather large (~ 0.5mm). This is because the liquid entrained at the prefilmer lip is rather slow and thick. We call this regime the "accumulation" regime. There is a strong change in the atomisation mechanism going along the vertical axis of increasing liquid injection velocity ($\overline{u}_{\mathrm{liq}} = 5 - 10$m/s). Only under higher liquid speeds does atomisation appear

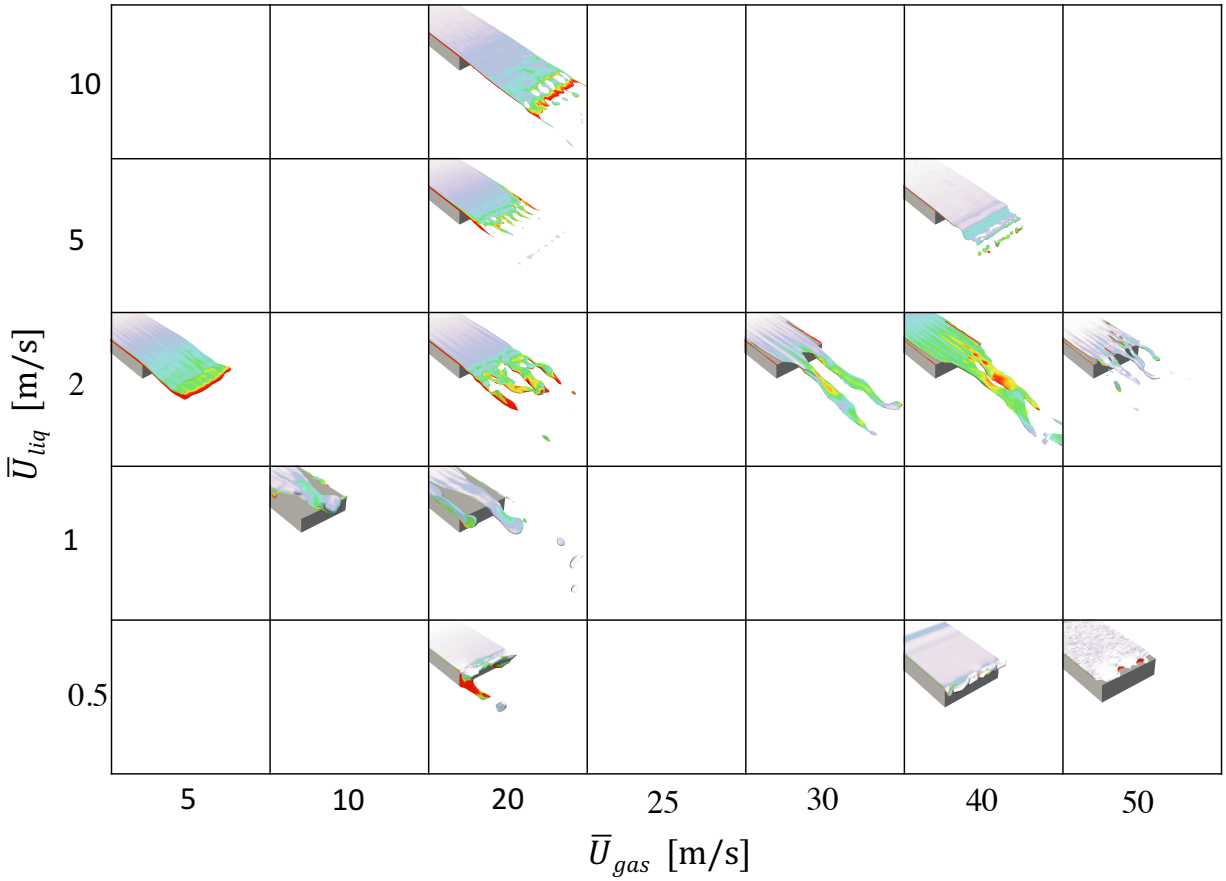

FIG. 3: Matrix representation of the observed liquid film breakup phenomena over our velocity parametric space. The iso-surface of ψ is shown, coloured by velocity magnitude.

to take place from the liquid sheet directly into such small droplets, whose diameter is as low as order 100μm. The observed regime was named "3-D wave mode". For a fixed liquid injection speed ($\overline{u}_{\mathrm{liq}} = 2$m/s) and increasing gas injection speed, the liquid suffers a diminished amplitude of interfacial distortion in the streamwise direction; only transverse wave modes are visible, in which surface tension forces dominate over aerodynamic forces leading to a "ligament-merging" behaviour. The droplets generated in this instance are rather large ($\sim$ 0.5mm). These observations are discussed in greater detail below.

Finally, for low liquid flow rates ($\overline{u}_{\mathrm{liq}} = 0.5$m/s) and high gas flow rates ($\overline{u}_{\mathrm{gas}} = 40 - 50$m/s), rim-driven retraction dynamics of a thickened film are observed. In Fig. 5b, one can observe the dewetting of the prefilmer imparted by a recession of the rim of the liquid film. The film retracts under the influence of the capillary force acting at its edge. It is combined with a perpendicular acceleration, which sets off a transverse instability, as described in Lhuissier and Villermaux (2011). The initially straight rim corrugates (Fig. 5a). Corrugation amplitudes grow, until they form rather regularly spaced deep indentations, ultimately forming cusps at the tip at which drops are released, much like in the "3D wave mode regime" and disintegration of streamwise ligaments (see Section 5.2). The formation of the rim instability driven by surface tension ressembles a Taylor–Culick instability for low Ohnesorge number (Oh$<$ 0.1) fluids (Savva and Bush, 2009).

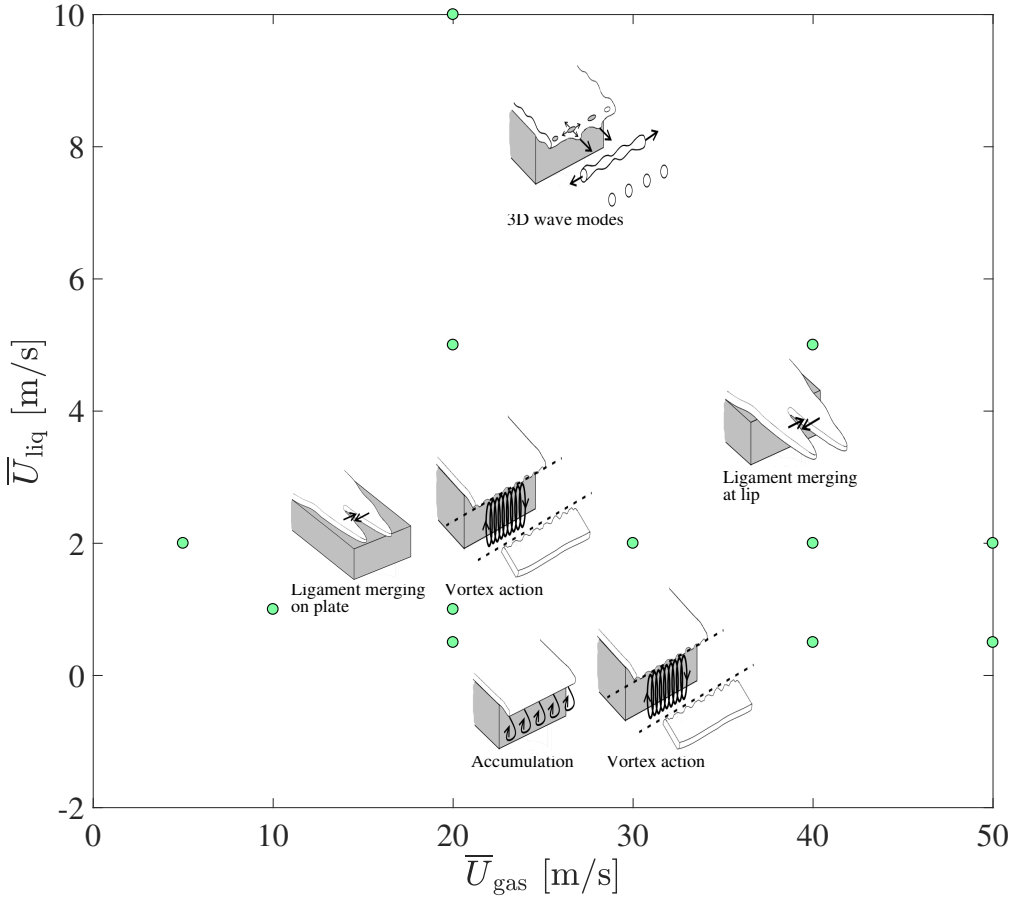

FIG. 4: Regime map obtained from our numerical simulation operating points (*green dots*) for prefilming liquid film atomisation.

5. MECHANISMS OF ATOMISATION

The breakup phenomena introduced in the previous section in an organised perspective – or cartography – are the consequence of a few physical mechanisms which are discussed in greater detail below.

5.1 Accumulation

The "accumulation" regime is located in the bottom-middle section of our cartography (Fig. 3). It is observed for low gas velocities of about $\overline{u}_{\mathrm{gas}} = 20$m/s. Fig. 6 shows a series of snapshots for the liquid film evolution with a bulk gas velocity of $\overline{u}_{\mathrm{gas}} = 20$m/s and $\overline{u}_{\mathrm{liq}} = 0.5$m/s. At 11.8ms (Fig. 6**a**), an initial cell-like structure – or membrane – starts forming. The growth of this modulation amplitude is the result of surface tension effects and shearing action of the gas exerted on the liquid. The membrane grows until it becomes of the order of the liquid film thickness and the film perforates at 14ms (Fig. 6**b**). This event is therefore accompanied by non-wetted regions on the prefilmer (visible in Fig. 6**b-c**). Membrane puncture has also been witnessed in the experimental works of Bremond et al. (2007), for example. The bursting of this membrane at 15ms upon the final rupture of its rim (Fig. 6**d**) builds the onset of primary breakup. A streamwise ligament forms that remains attached to the rim of the liquid film on the left hand side of the

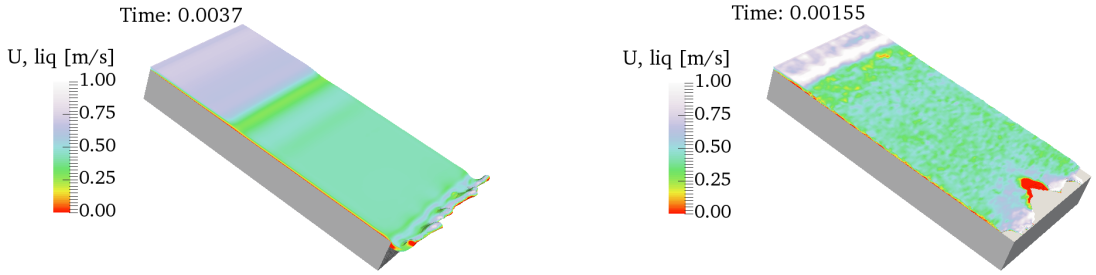

(a) $\overline{u}_{\mathrm{gas}} = 40$m/s and $\overline{u}_{\mathrm{liq}} = 0.5$m/s

(b) $\overline{u}_{\mathrm{gas}} = 50$m/s and $\overline{u}_{\mathrm{liq}} = 0.5$m/s

FIG. 5: Liquid film rim instability **(a)** and recession dynamics **(b)**, where red indicates negative velocities.

prefilmer, and a droplet detaches from the ligament through aerodynamic tearing (Fig. 6**e**). Following this first release of liquid, the liquid reservoir at the prefilmer lip is refilled and the whole process starts again (Fig. 6**f**).

We witness liquid attachment at the prefilmer lip via a meniscus (Fig. 6**d-f**), from which the streamwise ligament emerges. The formation of the meniscus is due to capillary action and is a well-known liquid behaviour for shear-driven flows over corner geometries (Bacharoudis et al., 2014). Accumulation is a well-documented atomisation regime, Fig. 7 shows side-by-side the similarity in the results from our numerical simulation with some backlit experimental images by Gepperth et al. (2012). This liquid wetting behaviour might change depending on the chosen substrate (wetting properties) and geometry: the effect of the thickness of the prefilmer trailing edge has been reported as influencing liquid attachment and accumulation Braun et al. (2015); Gepperth et al. (2012).

In the present atomisation regime, atomisation is limited to the close vicinity of the prefilmer lip. This represents an advantage when designing more compact combustion chambers. When atomisation is limited to a small and controlled area, the performance of the gas turbine is maximised. However, the present configuration yields droplets whose diameter exceeds the initial liquid film thickness.

The same accumulation phenomenon has previously been witnessed in the experiments of Gepperth et al. (2012), Inamura et al. (2012) and Déjean et al. (2016). Here, surface tension effects oppose any wave growth via inertial forces. As a consequence, this type of atomisation is said to be decoupled from any wave development appearing on the liquid film surface. A similar breakup phenomenon was observed by Gepperth et al. (2014) in annular airblast injectors, suggesting its relevance to real atomisers. The liquid attachment at the prefilmer lip via a meniscus (Lhuissier and Villermaux, 2011) is an important physical and chemical aspect to consider in the context of surface wetting behaviour and the subsequent atomisation mechanism. For example, Gepperth et al. (2014, 2012) only observed an atomisation mechanism of accumulation type. This might be due to their chosen range in operating conditions or linked to the use of an acrylic plastic prefilmer and the associated contact line hysteresis. However, the authors do not report on the level of hydrophobicity of that surface.

The thickness of the prefilmer trailing edge is a parameter influencing the level of accumulation of the liquid bulk (Gepperth et al., 2012), also dependent on the liquid film thickness. For prefilmer heights smaller than the average film thickness, the impact of the trailing edge has been reported to be reduced (Braun et al., 2015). For the manufacture of injection nozzles, this finding indicates that there is scope for the evaluation of substrate wetting comprising contact angle hysteresis in parallel with a change in prefilmer geometry.

5.2 3-D wave mode

The “3D wave mode” atomisation regime is located in the top section of our cartography in Fig. 3. The phase interface behaviour is subject to a high interfacial velocity shear, whereby rapidly growing surface waves – both longitudinal

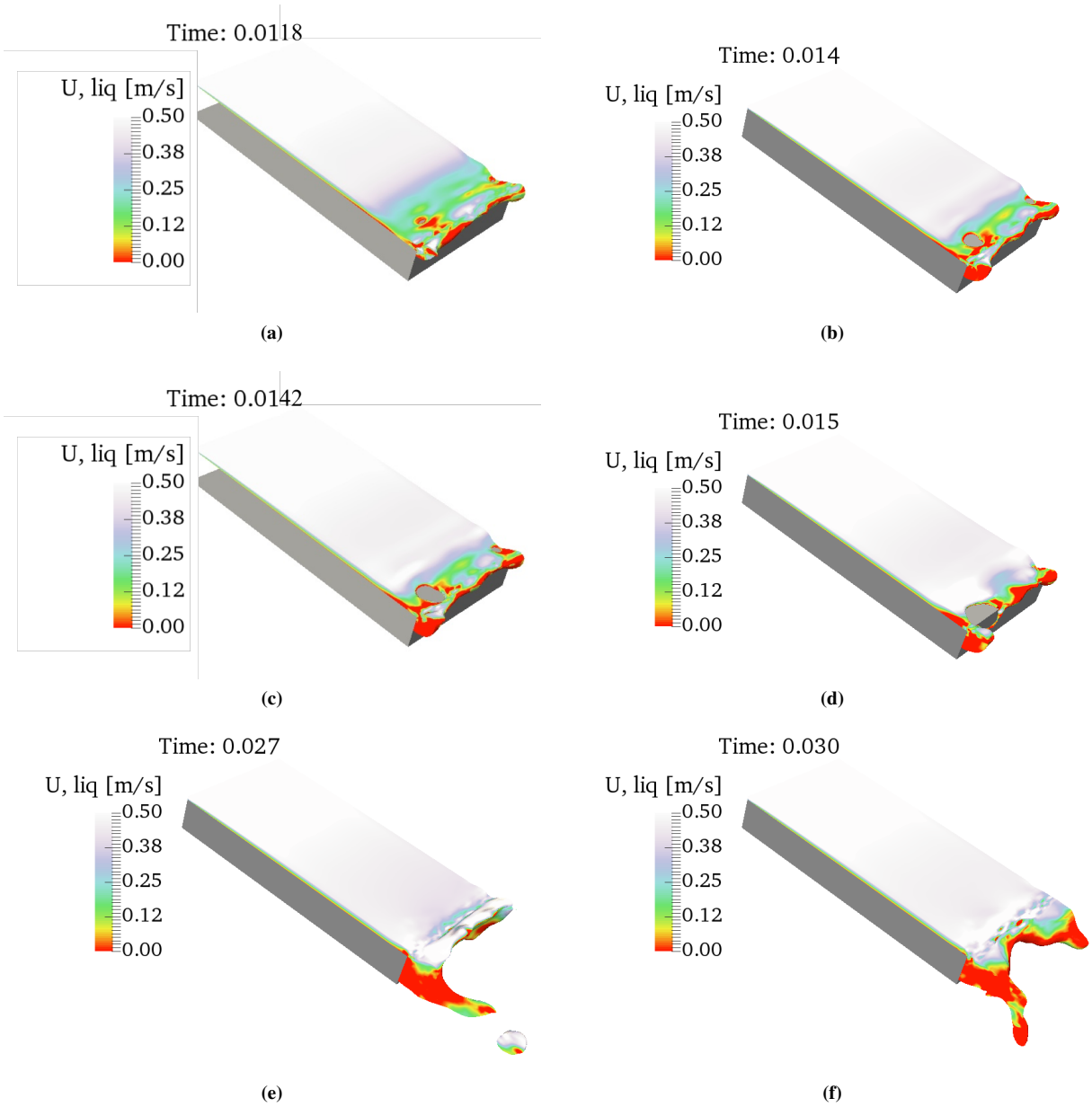

FIG. 6: Iso-surface of $\phi_\Gamma = 0.5$ coloured by liquid velocity for $\overline{u}_{\mathrm{gas}} = 20$m/s and $\overline{u}_{\mathrm{liq}} = 0.5$m/s showing the effect accumulation at the prefilmer trailing edge. Development of a membrane puncturing the liquid film **(a)** which breaks up **(b)** into a streamwise ligament that elongates and sheds a droplet into the air stream **(c-d)** before the liquid reservoir at the lip is refilled and the whole process starts again **(e-f)**.

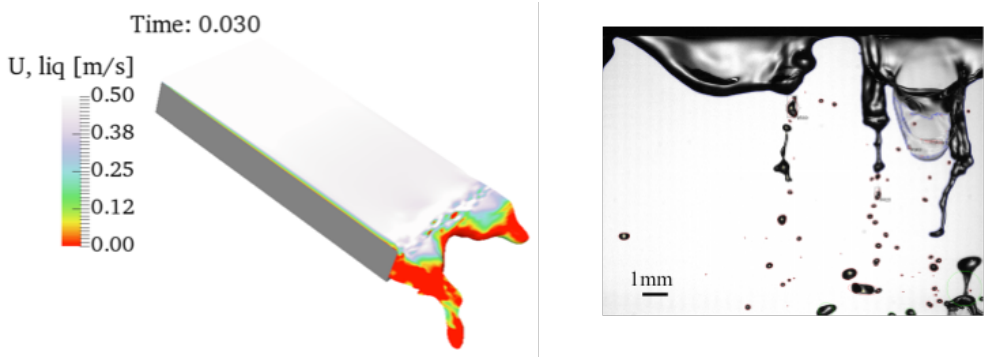

FIG. 7: Simulation result for the "accumulation" regime and backlit experimental image by Gepperth et al. (2012) side-by-side.

and transversal – are superimposed on the liquid film. Diverse liquid deformations originate through these hydrodynamic instabilities. We discern the development of a periodic variation of the sheet thickness. Instantaneous snapshots in Fig. 8 and Fig. 9 illustrate this behaviour. Fig. 10 shows side-by-side the similarity in the results from our numerical simulation at $\overline{u}_{\mathrm{gas}} = 20$m/s, $\overline{u}_{\mathrm{liq}} = 2$m/s with some backlit experimental images by Déjean et al. (2016).

Here, droplet formation results from the unstable growth of short wavelength surface waves on the surface. A clear distinction is made between spanwise and streamwise ligaments and their disintegration into smaller liquid structures under either aerodynamic tearing and/or in a way that resembles the Plateau–Rayleigh instability, as predicted by theoretical predictions (e.g. von Helmholtz, 1868) and experimental data (e.g. Bhayaraju and Hassa, 2009; Déjean et al., 2016). The droplets produced from the liquid surface have decreased significantly in size from the former "accumulation" atomisation regime. Indeed, for a fixed gas velocity at $\overline{u}_{\mathrm{gas}} = 20$m/s, an increasing liquid velocity from $\overline{u}_{\mathrm{liq}} = 0.5$m/s to 10m/s induces a lower interfacial velocity ratio. The ligaments formed are smaller in size, which leads to smaller drops being generated. As the mean gas velocity is increased from 20m/s (Fig. 8) to 40m/s (Fig. 9) – with $\overline{u}_{\mathrm{liq}}$ held constant at 5m/s, which corresponds to the top row of our cartography in Fig. 3 going from left to right – a higher amplitude sinuous mode develops on the liquid film and travels downstream, the film starts flapping, helping promote atomisation.

The tangential shearing forces act on the ligaments and cause them to be destabilised over rather short time periods and thus lead to early fragmentation. This is conducive to faster atomisation. However, since the liquid film is moving so fast, the liquid core rim has had time to reach the end of the prefilmer before the first atomisation events take place; the liquid film "shoots-off" the prefilmer trailing edge and atomisation happens many film thicknesses downstream. This spatial delay in the onset of atomisation is problematic with regards to jet-engine combustion.

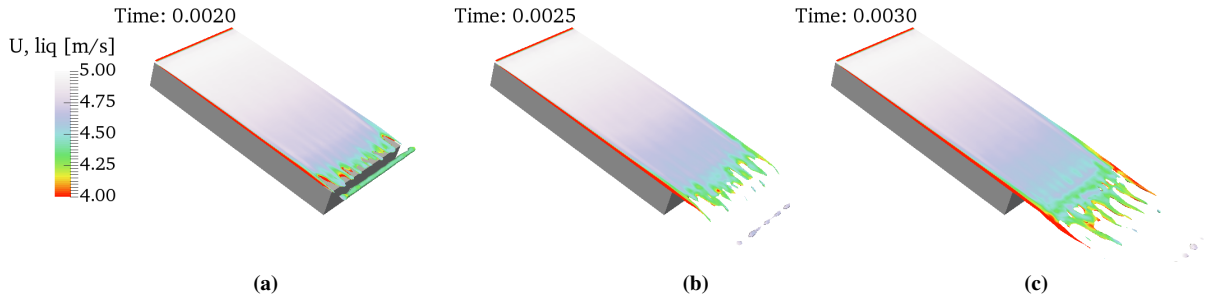

FIG. 8: Interface location coloured by liquid velocity for $\overline{u}_{\mathrm{gas}} = 20$m/s, $\overline{u}_{\mathrm{liq}} = 5$m/s. First, a transverse roll ruptures into drops under capillary breakup, followed by the formation and elongation of longitudinal ligaments and their pinch-off.

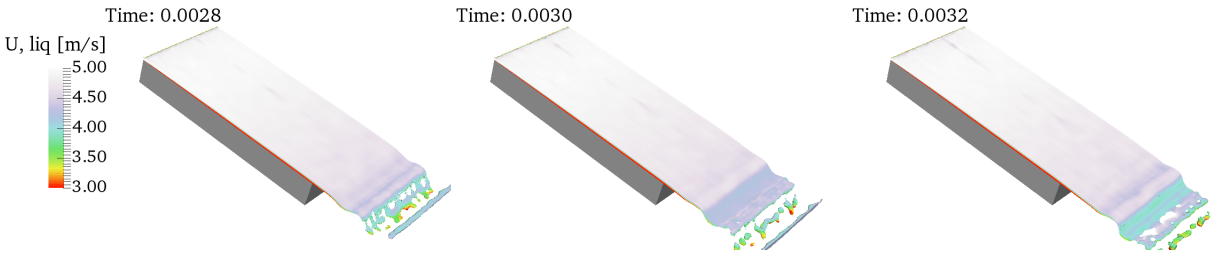

FIG. 9: Interface location coloured by liquid velocity for $\overline{u}_{\rm gas} = 40$m/s, $\overline{u}_{\rm liq} = 5$m/s. Membrane puncturing and formation of transverse ligaments that rupture into drops under capillary breakup.

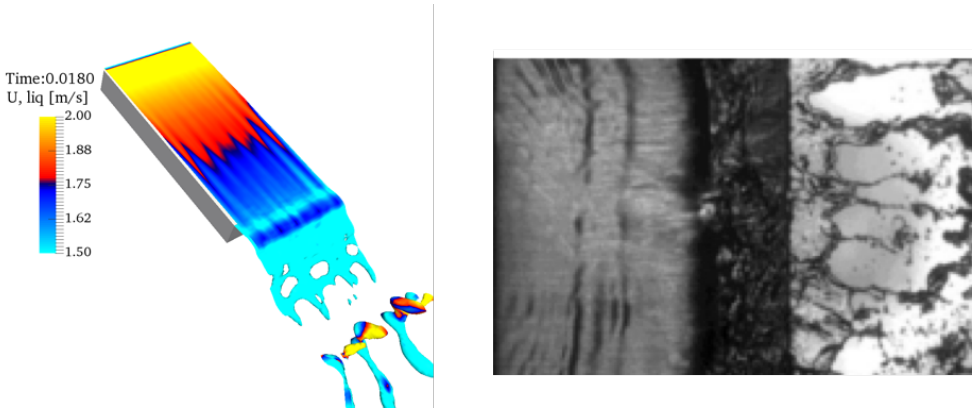

FIG. 10: Simulation result at $\overline{u}_{\rm gas} = 20$m/s, $\overline{u}_{\rm liq} = 2$m/s showing longitudinal and transverse waves breaking into ligaments, and backlit experimental image by Déjean et al. (2016) side-by-side.

5.3 Ligament merging

For a fixed liquid injection velocity of 2m/s, the mean gas velocity was varied spanning a range from 5m/s to 50m/s, which correspond to a parabolic profile centreline velocity of 10m/s to 100m/s. Longitudinal instabilities seem not to have an impact on the thickness modulation of the liquid film. They are visible through the velocity field mapped on to the liquid/vapour interface contour (Fig. 11). The high-speed gas co-flow seems to constrain the growth of sinusoidal longitudinal waves, a comment also made by Lozano and Barreras (2001).

On the other hand, transverse waves do induce thickness modulations from which liquid structures elongated in the streamwise direction emerge. As more liquid is injected, it feeds the growth of these long streamwise ligaments, which merge and pair up over time, as depicted in Fig. 12. As the ligaments reach out for the prefilmer lip, they remain attached to it and break up by pinching off the remaining liquid bulk. A similar ligament-merging behaviour occurs for smaller mean gas velocities and a fixed liquid injection velocity of 1m/s (Fig. 13). The result from such a pairing up process is that droplet sizes tend to be larger. In this atomisation regime, the surface tension forces dominate over the inertia forces. Considering that the liquid stream is not fully wetting the prefilmer, these results might be of high relevance for other applications such as the surface treatment of substrates, in which wetting with washing or etching liquids is critical (Yarin, 2006).

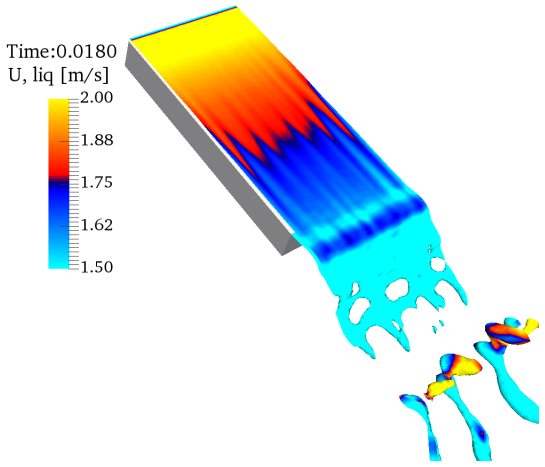

FIG. 11: Interface location coloured by liquid velocity for $\overline{u}_{\mathrm{gas}} = 20$m/s and $\overline{u}_{\mathrm{liq}} = 2$m/s showing the longitudinal wavelengths.

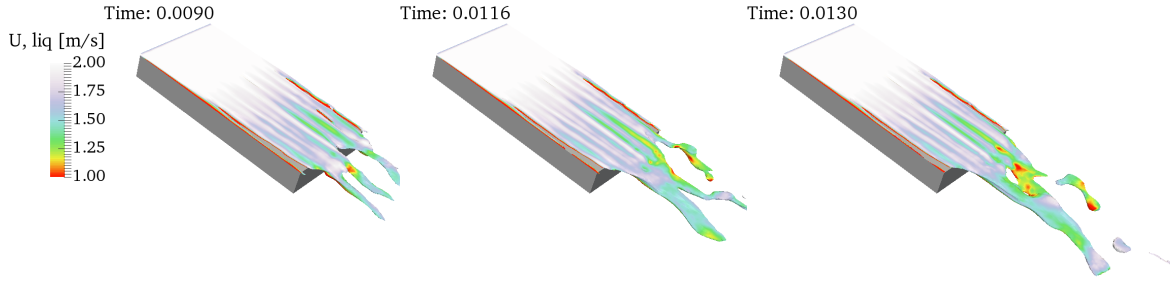

FIG. 12: Interface location coloured by liquid velocity for $\overline{u}_{\mathrm{gas}} = 40$m/s and $\overline{u}_{\mathrm{liq}} = 2$m/s showing the ligament-merging dynamics encountered for an increasing gas injection velocity at the prefilmer lip.

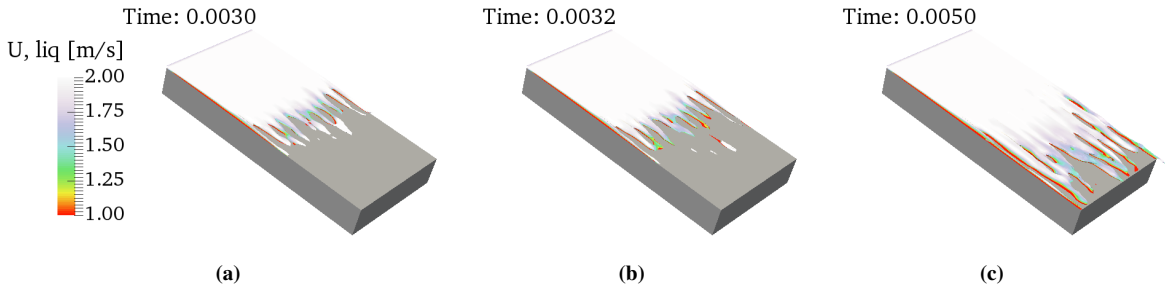

FIG. 13: Interface location coloured by liquid velocity for $\overline{u}_{\mathrm{gas}} = 50$m/s and $\overline{u}_{\mathrm{liq}} = 2$m/s showing the ligament-merging dynamics as they evolve on the prefilmer plate.

5.4 Vortex action

Another vehicle for atomisation comes through the action of gas vortices on the liquid film. The vortices in the gas stream are interacting with the flapping interface such that once the liquid film has passed the atomiser lip and is supported by the two co-flow gas streams, vortex rotation is influencing either the lower or the upper side of the liquid surface. When the liquid film bends upwards, pushed from below by a vortex core, and obstructs the gas stream (Fig. 14), it is exposed to relatively high aerodynamic forces, which promote primary breakup. Similarly, as a gas vortex forms in the top gas channel thus affecting the upper side of the sheet, it causes the tip of the liquid film to bend upward and the trough of the wave downwards, before the entire structure is separated from the remaining liquid stream (Fig. 15). We named this wavy sheet atomisation mechanism, "vortex action". It has been witnessed by several experimentalists for both non-prefilming (Fraser et al., 1962; Villermaux and Clanet, 2002) and prefilming configurations (Bhayaraju and Hassa, 2009). Agbaglah et al. (2015) and Fuster et al. (2009) also noted the intense and extended gas vortices generated that interact with the liquid bulk, and indicated that the fluctuations in the gas stream play an important role in the breakup of the liquid.

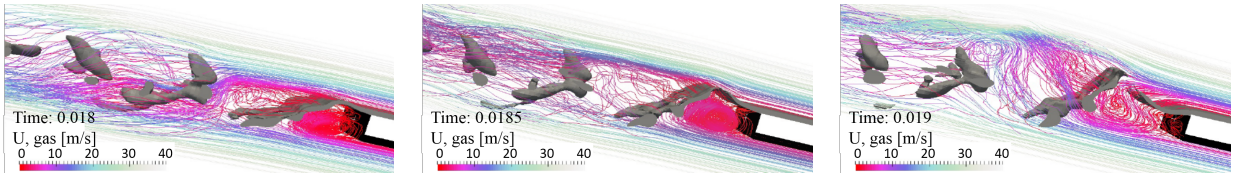

(a) **(b)** **(c)**

FIG. 14: Air streamlines revolving around the liquid bulk. Flapping is promoting atomisation. $\overline{u}_{\mathrm{gas}} = 20$m/s, $\overline{u}_{\mathrm{liq}} = 2$m/s.

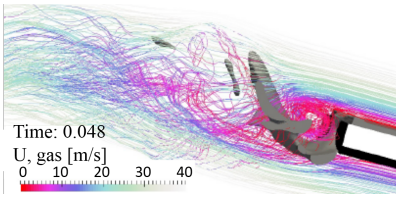

FIG. 15: Disintegration by vortex action. A strong vortex core is coming from the top gas channel. $\overline{u}_{\mathrm{gas}} = 20$m/s, $\overline{u}_{\mathrm{liq}} = 0.5$m/s.

6. DISCUSSION

6.1 Competing for inertia: behaviour at the prefilmer lip

The present simulations have also highlighted the sensitivity of the breakup mode to the evolution of the two-phase flow downstream of the trailing edge. The latter is largely conditioned by the relative inertia of the gas and the liquid. On one hand, the high aerodynamic forces imparted by the gas on the liquid film can dictate the liquid evolution, such as when vortex action is part of the breakup process, during which the gas is able to displace the liquid film despite its large inertia. For example, as part of the accumulation regime, the vortex rotation in the recirculation zone close to the prefilmer lip affects the liquid surface and acts to promote the observed intermittent liquid release. Here, the liquid film is prone to the inertia forces exerted by the gas on each side of its surface. The combination of vortex action (gas inertia-driven) and accumulation (liquid inertia-driven and surface tension driven), appear to act together to destabilise the liquid film at the trailing edge.

On the other hand, the high inertia of the liquid film can dominate over that of the gas and impart interfacial dynamics obeying intrinsic surface tension forces. Indeed, although the liquid occupies a smaller volume in comparison

to the gas channels, and has a lower mean velocity, it is approximately a thousand times denser, hence has a major impact on the mass flow rate.

For instance, the arrival of the liquid film at the prefilmer lip induces a re-arrangement of the entire cross-sectional gas/liquid velocity profile. The unsteady wake behind the atomiser edge (similar to von Kármán vortex streets) is suppressed and the regularity of the velocity variation is lost. This shows the coupled character between the liquid film and the vortex dynamics of the gas flow, confined in the long narrow primary breakup region, and the dominance of the high inertia of the liquid film in the fluid dynamics.

In fact, as the liquid film gets faster (in the 3-D wave mode regime), it concentrates more and more momentum in the x-direction. Thus, any deviation in the movement of the liquid film perpendicular to the x-direction is effectively suppressed. The gas adapts itself around the liquid film. At the prefilmer lip, a stagnation zone of zero gas velocity co-exists with the liquid film gliding over it. The size of the recirculation zone changes depending on the length of the intact liquid film downstream of the lip (Fig. 16). Again, this response to confinement of the recirculation zone is due to the relative inertia of the two fluids, in favour of the liquid. A similar conclusion in the ligament-merging regime is supported by the observation that the inertia in the streamwise direction is mainly concentrated within the liquid and that the gas is being "pushed around" to make way for the liquid.

6.2 Liquid surface tension-driven mechanisms

Overall, based on the observed atomisation behaviour, the development of the liquid film on the prefilmer plate can locally be dictated by the combination of two physical forces: aerodynamic action (vortex action, membrane puncturing, ligament disintegration) and liquid surface wetting set by surface tension effects, which seem to play a major role in the atomisation process. Indeed, in the ligament-merging regime, the strong intrinsic liquid surface tension force prevents airblast atomisation by holding the liquid together. In the accumulation regime, the capillary forces seem to play a role in liquid attachment at the prefilmer lip and the subsequent atomisation pattern. Finally, in the bottom-right corner of our cartography, under the influence of capillarity, rim-retraction dynamics appear to destabilise the liquid film.

6.3 Shearing ratio versus momentum flux ratio

Our simulations have reproduced the series of instabilities, leading to the formation of ligaments, as mechanisms for the disintegration of those ligaments into droplets. This conveys the importance of viscous shearing at the phase-interface between the two fluids, which will have a major influence on the occurrence and scales of these instabilities. Chaussonnet (2014) noted the importance of shear stress. Furthermore, he postulated that neglecting surface wave development considerably modified the liquid film velocity and locally impacted the wall shear stress prediction. In addition, the shear stress force exerted by the gas on the liquid surface depends on the slope of the velocity profile and the difference in viscosities (Fig. 17). Indeed, a previous study revealed the formation of backwards running waves owing to a change in shear stress forces (Bilger and Cant, 2014).

Despite the recognised importance of the interfacial shearing ratio, there is a widespread postulate that considers the momentum flux ratio (MFR) to be one of the determining factor in classifying atomisation regimes (Gepperth et al., 2014; Warncke et al., 2017). There seems to be a common agreement that higher aerodynamic forces, through a higher MFR or a higher aerodynamic relative Weber number, are always synonymous with an enhancement in atomisation quality (e.g. Bhayaraju and Hassa, 2009; Fernandez et al., 2009; Inamura et al., 2012), i.e. the formation of smaller droplets.

In the present work, we see no monotonic dependence of the atomisation quality with inertia ratio. The MFR or Weber number is not sufficient to distinguish the prevalence of one atomisation mechanism from another. For example, moving upward on the regime cartography of Fig. 3, we observe the "3D wave mode regime" with the generation of very small droplets. However, this corresponds to a lower Weber number (reduced relative velocity between the two fluids). In addition, for an increase in gas velocity, the ligament-merging regime is governed by a high liquid inertia and surface tension forces accompanied by the generation of larger liquid droplets.

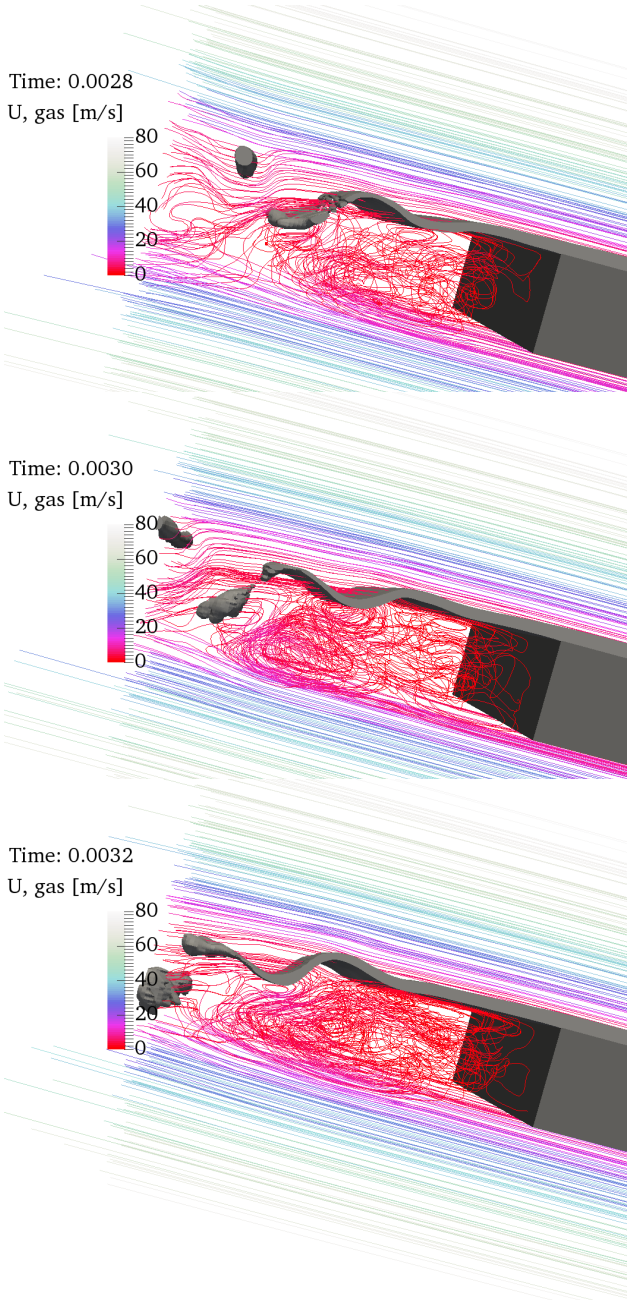

FIG. 16: Recirculation zone underneath the liquid film for $\overline{u}_g = 40$m/s and $\overline{u}_l = 5$m/s. The liquid inertia wins over the air displacement.

Such apparent contradictions are not surprising, since there is as yet no universal consensus regarding which fluid parameters and geometrical parameters characterise the breakup process in liquid film configurations and direct the classification of atomisation regimes. For example, Déjean et al. (2016) incorporated the strong influence of the prefilmer plate length as well as vorticity layer thickness into their non-dimensional regime cartography, effectively including the influence of the shear stress ratio discussed earlier as well as the MFR.

In light of the present numerical results, we propose the following interpretation. The dominant influence of the interfacial shear was illustrated by the "3D wave mode" atomisation regime involving liquid destabilisation into small droplets for high liquid and high gas velocities. On the other hand, at the prefilmer trailing edge, certain atomisation mechanisms, such as "ligament-merging" and "accumulation" as well as the rim-retraction dynamics, are dominated by the influence of liquid inertial forces.

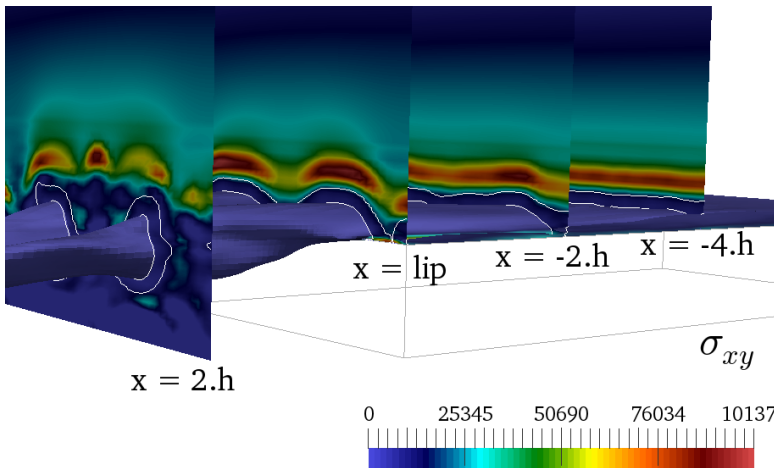

FIG. 17: Iso-surface of $\psi_\Gamma = 0.5$ for $\overline{u}_g = 30$m/s and $\overline{u}_l = 2$m/s and 2-D slices at different prefilmer height h locations in the x-direction coloured by shear stress ($\sigma_{xy} = \dfrac{\partial u_x}{\partial y}$).

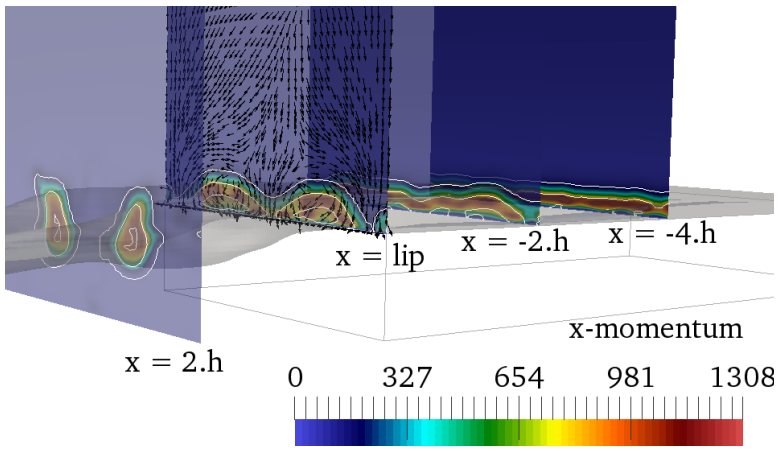

FIG. 18: Iso-surface of $\psi_\Gamma = 0.5$ for $\overline{u}_g = 30$m/s and $\overline{u}_l = 2$m/s and 2-D slices at different prefilmer height h locations in the x-direction coloured by momentum (ρu^2).

7. FINAL REMARKS

Current understanding of liquid film fragmentation is incomplete and only partially correlated to the available experimental results, as the data are either too scattered or obtained over insufficient ranges of varied parameters. This state of affairs provides an opportunity for continuing to investigate the physics for several operating conditions.

The objective of this study was therefore twofold: to extract information on interfacial dynamics and atomisation mechanisms following a consistent fundamental investigation of the physics in velocity space, and offer a reasoned regime cartography for liquid film atomisation. We were able to draw several conclusions about the description of the liquid phase in the dense spray region of prefilming airblast atomisers and to develop an original approach to classify them. It is found that, for some operating conditions, the primary breakup mechanism of the liquid film is rather different from that indicated by well-established theories on classical liquid sheet breakup on prefilming surfaces. An evaluation of the theories shows that aerodynamic effects alone are not sufficient to explain the observed behaviour. However, mechanisms that combine liquid-gas aerodynamic interaction with surface tension effects and inertial differences provide a better description. New regime-dependent insights are observed into the physics of liquid film behaviour, for instance, phenomena like "ligament-merging" or the liquid rim subjected to a Taylor–Culick-like instability. In addition, three-dimensional wave modes were observed to co-exist and work together to destabilise the liquid film ("3-D wave mode" regime). Accumulated liquid at the atomising edge undergoes deformation by which droplets are generated ("accumulation" regime). Finally, "vortex action" is another observed mechanism by which the liquid film is fragmented. All of these key physical atomisation mechanisms have been mapped out. The proposed cartography helps to predict the evolution of the atomisation process according to the operating conditions of the injection system. The effect of the liquid and gas velocities appear to be strongly regime-dependent, highlighting the need to continue investigating the physics in different regimes.

Furthermore, it should be noted that in real applications the two gas streams that interact with the liquid film are usually characterised by different velocities and swirling rotations. This aspect is not considered in the numerical investigations described here and its impact on the atomisation process and on the distribution of droplets between the two flows remains to be characterised.

During the course of this research project, it became apparent that the study of dynamic wetting behaviours of liquid films on dry solid substrates would be important. The addition of a reliable model for the accurate estimation of the contact-line forces is paramount. Especially for the prediction of any receding dynamics of the liquid film, or atomisation at corner edges (Bacharoudis et al., 2014). Thus, the RCLS method was further developed to include a dynamic contact angle model, which is being validated against experimental data for the simulation of droplet splashing on a dry hydrophobic surface. The latter is the subject of a paper in preparation.

The RCLS method provides the fidelity needed to capture the dynamics of the phase interface and isolated liquid droplets accurately. It will be interesting in the future to extract quantitative information from the present results on droplet size and velocity distribution. A droplet recognition, tracking and transfer algorithm was implemented within our numerical method. A quantitative validation would provide a useful follow-up assessment of the performance of the present numerical tool. A small number of state-of-the-art techniques to image spray formation in optically dense regions of atomising sprays have appeared in the literature (Arienti et al., 2011; Guildenbecher, 2016, e.g.). The data from these new diagnostics will be useful for development and validation of our numerical tool.

ACKNOWLEDGMENTS

This work was funded by Rolls-Royce Group plc and EPSRC. The authors would like to thank Pierre Roy for his valuable input in graphic design.

DECLARATION

The authors confirm that this article has not been published elsewhere and has not been simultaneously submitted for publication elsewhere.

REFERENCES

Agbaglah, G.G., McCaslin, J., and Desjardins, O., Numerical simulations of air-blast atomization of a liquid layer, *Proceedings of the* 27^{th} *Annual Conference of the Institute for Liquid Atomization and Spray Systems – ILASS Americas*, Raleigh, North-Carolina, 2015.

Arienti, M., Wang, L., Corn, M., Li, X., Soteriou, M.C., Shedd, T.A., and Herrmann, M., Modeling Wall Film Formation and Breakup Using an Integrated Interface-Tracking/Discrete-Phase Approach, *ASME Journal of of Engineering for Gas Turbines and Power*, vol. **133**, pp. 031501–1, 2011.

Bacharoudis, E., Bratec, H., Keirsbulck, L., Buchlin, J.M., and Labraga, L., Simplified model for the prediction of the occurrence of film atomization in corner geometries, *International Journal of Multiphase Flow*, vol. **58**, pp. 325–337, 2014.

Bhayaraju, U. and Hassa, C., Planar liquid sheet breakup of prefilming and nonprefilming atomizers at elevated pressures, *Atomization and Sprays*, vol. **19**, pp. 1147–1169, 2009.

Bianchi, G.M., Pelloni, P., Toninel, S., Scardovelli, R., Leboissetier, A., and Zaleski, S., Improving the Knowledge of High-Speed Liquid Jets Atomization by Using Quasi-Direct 3D Simulation, *SAE Technical Paper*, 2005-24-089, 2005.

Bilger, C., Aboukhedr, M., Vogiatzaki, K., and Cant, R.S., Evaluation of two-phase flow solvers using Level Set and Volume of Fluid methods, *Journal of Computational Physics*, vol. **345**, pp. 665–686, 2017.

Bilger, C. and Cant, R.S., Numerical investigation of shear-driven liquid film primary breakup assisted by coaxial gas streams, *Proceedings of the* 26^{th} *Annual Conference on Liquid Atomization and Spray Systems – ILASS Europe*, Bremen, Germany, 2014.

Brackbill, J., Kothe, D., and Zemach, C., A continuum method for modeling surface tension, *Journal of Computational Physics*, vol. **100**, pp. 335–354, 1992.

Braun, S., Wieth, L., Koch, R., and Bauer, H.J., Influence of Trailing Edge Height on Primary Atomization: Numerical Studies Applying the Smoothed Particle Hydrodynamics (SPH) Method, *Proceedings of the* 13^{th} *Triennial International Conference on Liquid Atomization and Spray Systems – ICLASS*, Tainan, Taiwan, 2015.

Bremond, N., Clanet, C., and Villermaux, E., Atomization of undulating liquid sheets, *Journal of Fluid Mechanics*, vol. **585**, pp. 421–456, 2007.

Chaussonnet, G., Modeling of liquid film and breakup phenomena in Large-Eddy Simulations of aeroengines fueled by airblast atomizers, PhD thesis, Institut National Polytechnique de Toulouse, 2014.

Cuenot, B., Vicquelin, R., Riber, E., Moureau, V., Lartigue, G., Figuer, A., Mery, Y., Lamouroux, J., Richard, S., Gicquel, L., Schmitt, T., and Candel, S., Advanced Simulation of Aeronautical Combustors, *Journal Aerospace Lab*, vol. **11**, pp. 1–9, 2016.

de Villiers, E., Gosman, A., and Weller, H., Large eddy simulation of primary diesel spray atomization, *SAE Technical Paper*, 2004-01-0100, 2004.

Déjean, B., Etude expérimentale de l'atomisation d'une nappe liquide avec et sans zone de pré-film en vue de sa modélisation – Influence des conditions limites, PhD thesis, Institut Supérieur de l'Aéronautique et de l'Espace (ISAE), 2015.

Déjean, B., Berthoumieu, P., and Gajan, P., Experimental study on the influence of liquid and air boundary conditions on a planar air-blasted liquid sheet, part ii: prefilming zone length., *International Journal of Multiphase Flow*, vol. **79**, pp. 214–224, 2016.

Desjardins, O., Numerical methods for liquid atomization and application in detailed simulations of a diesel jet, PhD thesis, Stanford University, 2008.

Faeth, G.M., Hsiang, L.P., and Wu, P.K., Structure and breakup properties of sprays, *International Journal of Multiphase Flow*, vol. **21**, pp. 99–127, 1995.

Fernandez, V., Berthoumie, P., and Lavergne, G., Liquid sheet disintegration at high pressure: An experimental approach, *Comptes Rendus Mécanique*, vol. **337**, pp. 481–491, 2009.

Fraser, R.P., Eisenklam, P., Dombrowski, N., and Hasson, D., Drop formation from rapidly moving liquid sheets, *AIChE Journal*, vol. **8**, pp. 672–680, 1962.

Fuster, D., Bagué, A., Boeck, T., Le Moyne, L., Leboissetier, A., Popinet, S., Ray, P., Scardovelli, R., and Zaleski, S., Simulation of primary atomization with an octree adaptive mesh refinement and VOF method, *International Journal of Multiphase Flow*, vol. **35**, pp. 550–565, 2009.

Gepperth, S., Bärow, E., Koch, R., and Bauer, H., Primary atomization of prefilming airblast nozzles: Experimental studies using advanced image processing techniques, *Proceedings of the 26$^{\mathrm{th}}$ Annual Conference on Liquid Atomization and Spray Systems – ILASS Europe*, Bremen, Germany, 2014.

Gepperth, S., Guildenbecher, D., Koch, R., and Bauer, H.J., Ligament and Droplet Characteristics in Prefilming Airblast Atomization, *12$^{\mathrm{th}}$ Triennial International Conference on Liquid Atomization and Spray Systems*, Institute for Liquid Atomization and Spray Systems, Heidelberg, Germany, 2012.

Guildenbecher, D.R., Recent Developments in Experimental Methods for Quantification of High-speed, Aerodynamically Driven Liquid Breakup, *Proceedings of the* 28$^{\mathrm{th}}$ *Annual Conference of the Institute for Liquid Atomization and Spray Systems – ILASS Americas*, Detroit, MI, 2016.

Guildenbecher, D.R., López-Rivera, C., and Sojka, P.E., Secondary atomization, *Experiments in Fluids*, vol. **46**, pp. 371–402, 2009.

Inamura, T., Shirota, M., Tsushima, M., Kato, M., Hama-jima, S., and Sato, A., Spray Characteristics of Prefilming Type of Airblast Atomizer, *Proceedings of the* 12$^{\mathrm{th}}$ *Triennial International Conference on Liquid Atomization and Spray Systems – ICLASS*, Heidelberg, Germany, 2012.

Issa, R., Solution of the implicitly discretised fluid flow equations by Operator-Splitting, *Journal of Computational Physics*, vol. **62**, pp. 40–65, 1985.

Kane, J.H., *Boundary element analysis*, Englewood Cliffs, NJ: Prentice Hall, 1994.

Kim, D. and Moin, P., Numerical simulation of the breakup of a round liquid jet by a coaxial flow of gas with a subgrid Lagrangian breakup model, *Center for Turbulence Research Annual Research Briefs*, pp. 15–30, 2011.

Lefebvre, A.H., *Atomization and Sprays*, Hemisphere Publishing Corporation, New-York, 1989.

Levich, V., *Physicochemical Hydrodynamics*, Prentice-Hall, Englewood Cliffs, NJ, 1962, pp. 636–546.

Lhuissier, H. and Villermaux, E., The destabilization of an initially thick liquid sheet edge, *Physics of Fluids*, vol. **23**, pp. 1–4, 2011.

Ling, Y., Fuster, D., Zaleski, S., and Tryggvason, G., Spray formation in a quasiplanar gas-liquid mixing layer at moderate density ratios: A numerical closeup, *Physical Review Fluids*, vol. **2**, p. 014005, 2017.

Lozano, A. and Barreras, F., Experimental study of the gas flow in an air-blasted liquid sheet, *Experiments in Fluids*, vol. **31**, pp. 367–376, 2001.

Lozano, A., Barreras, F., Siegler, C., and Löw, D., The effects of sheet thickness on the oscillation of an air-blasted liquid sheet, *Experiments in Fluids*, vol. **39**, pp. 127–139, 2005.

Lozano, A., Calvo, E., García, J.A., and Barreras, F., Mode transitions in an oscillating liquid sheet, *Physics of Fluids*, vol. **23**, pp. 044–103, 2011.

Marmottant, P. and Villermaux, E., On spray formation, *Journal of Fluid Mechanics*, vol. **498**, pp. 73–111, 2004.

Olsson, E. and Kreiss, G., A conservative level set method for two phase flow, *Journal of Computational Physics*, vol. **210**, pp. 225–246, 2005.

Olsson, E., Kreiss, G., and Zahedi, S., A conservative level set method for two phase flow II, *Journal of Computational Physics*, vol. **225**, pp. 785–807, 2007.

Pringuey, T., Large Eddy Simulation of Primary Liquid-Sheet Breakup, PhD thesis, University of Cambridge, Department of Engineering, 2012.

Pringuey, T. and Cant, R.S., High order schemes on three-dimensional general polyhedral meshes – application to the level set method, *Communications in Computational Physics*, vol. **12**, pp. 1–41, 2012.

Pringuey, T. and Cant, R.S., Robust Conservative Level Set method for 3D mixed-element meshes – Application to LES of primary liquid-sheet breakup, *Communications in Computational Physics*, vol. **16**, pp. 403–439, 2014.

Sauer, B., Direct numerical simulation of the primary breakup of aircraft engine related two-phase flows, PhD thesis, Technischen Universität Darmstadt, 2014.

Sauer, B., Sadiki, A., and Janicka, J., Embedded dns concept for simulating the primary breakup of an airblast atomizer, *Atomization and Sprays*, vol. **26**, pp. 187–215, 2016.

17 Savva, N. and Bush, J.W.M., Viscous sheet retraction, *Journal of Fluid Mechanics*, vol. **626**, pp. 211–240, 2009.

18 Som, S. and Aggarwal, S., Effects of primary breakup modeling on spray and combustion characteristics of compression ignition
546 engines, *Combustion and Flame*, vol. **157**, pp. 1179–1193, 2010.

547 Sussman, M., Smereka, P., and Osher, S., A level set approach for computing solutions to incompressible two-phase flow, *Journal*
548 *of Computational Physics*, vol. **114**, pp. 146–159, 1994.

549 Taylor, G., 1963. Generation of ripples by wind blowing over a viscous liquid, *The Scientific Papers of Sir Geoffrey Ingram Taylor*
550 *Vol. 3*. Batchelor, G. (Ed.). Cambridge University Press, Ch. 25, pp. 244–254.

551 Villermaux, E. and Clanet, C., Life of a flapping liquid sheet, *Journal of Fluid Mechanics*, vol. **462**, pp. 341–363, 2002.

552 von Helmholtz, H.L.F., On the discontinuous movements of fluids, *Monthly Reports of the Royal Prussian Academy of Philosophy*
553 *in Berlin*, vol. **23**, pp. 215–228, 1868.

554 Warncke, K., Gepperth, S., Sauer, B., Sadiki, A., Janicka, J., Koch, R., and Bauer, H.J., Experimental and numerical investigation
555 of the primary breakup of an airblasted liquid sheet, *International Journal of Multiphase Flow*, vol. **91**, pp. 208–224, 2017.

556 Weller, H.G., Tabor, G., Jasak, H., and Fureby, C., A tensorial approach to computational continuum mechanics using object-
557 oriented techniques, *Journal of Computational Physics*, vol. **12**, pp. 620–631, 1998.

558 Yarin, A., Drop impact dynamics: Splashing, Spreading, Receding, Bouncing, *Annual Review of Fluid Mechanics*, vol. **38**, pp. 159–
559 192, 2006.

560 Zuzio, D., Estivalèzes, J.L., and DiPierro, B., An improved multiscale Eulerian–Lagrangian method for simulation of atomization
561 process, *Computational Science & Discovery*, 2017, dOI 10.1016/j.compfluid.2016.12.018.